A strategy for designing microencapsulated composite phase change thermal storage materials with tunable melting temperature

Haiting Wei[a], Cuiping Wang[a,*], Shuiyuan Yang[a], Jiajia Han[a], Mujin Yang[a], Jinbin Zhang[a], Yong Lu[a], Xingjun Liu[b,c,d,**]

[a] College of Materials and Fujian Provincial Key Laboratory of Materials Genome, Xiamen University, Xiamen, 361005, PR China
[b] State Key Laboratory of Advanced Welding and Joining, Harbin Institute of Technology, Shenzhen, 518055, PR China
[c] Institute of Materials Genome and Big Data, Harbin Institute of Technology, Shenzhen, 518055, PR China
[d] Shenzhen R&D Center for Al-based Hydrogen Hydrolysis Materials, Shenzhen, 518055, PR China

ARTICLE INFO

ABSTRACT

Thermal energy storage technology with high temperature phase change materials (PCMs) plays an increasingly important role in the concentrated solar power plants and industrial waste heat recovery systems. In this study, a novel displacement reaction between tetraethoxysilane as SiO_2 source and molten raw Al powder was purposed to successfully prepare Al-Si/Al_2O_3 high temperature composite PCMs. Interestingly, by proposed synthetic methodology, we not only achieved the in-situ synthesis of Al-Si alloy PCM and Al_2O_3 shell, but also realized the controllability of Al-Si alloy composition and Al_2O_3 shell layer thickness. Our results indicated that the melting temperature of the prepared composite PCMs depended on the composition of Al-Si alloy, and could be designed within a certain temperature range (from 574.0 °C to 641.4 °C), instead of a particular temperature point. The melting temperature adjustability of the prepared composite PCMs provided an additional flexibility in different working temperature conditions. Moreover, the prepared composite PCMs exhibited a relatively high thermal storage capacity (248.6 J/g to 331.0 J/g), good thermal stability, excellent repeatable utilization property and certain shell layer self-repairing ability in the working temperature range. Therefore, the prepared composite PCMs can prove to be promising thermal energy storage materials for improving the energy efficiency in various systems under different working temperature conditions.

1. Introduction

With a rapid development in science and technology, the global problems of environment pollution and energy shortage have increased sharply. In order to alleviate these problems, it is necessary to develop the sources of renewable energy and improve their energy efficiency [1–3]. Thermal energy storage technology plays a vital role in the high efficiency energy utilization of concentrated solar power plants and various industrial systems. Phase change materials (PCMs) used for thermal energy storage have drawn an increasing public attention owing to their small temperature variation from storage to release, high thermal energy storage density and repeatable utilization property [4–7].

Molten salts with the melting temperature over 500 °C, including sulfate [8], carbonate [9] and chloride [10], are the most studied high temperature PCMs due to their high thermal energy storage density.

However, the thermal conductivity of molten salts is too poor (e.g. KNO_3: $0.5 Wm^{-1}K^{-1}$ [11]) to realize the rapid and efficient thermal storage and release. Many efforts have been made in this regard, like dispersing carbon fibers or metal particles with high thermal conductivity in the PCM matrix, to enhance the thermal conductivity of molten salts PCMs [12,13]. Nevertheless, it is inevitable to improve the thermal conductivity at the expense of thermal storage density. Additionally, the high volume expansion ratio (e.g. NaCl: 25.58% [5]) makes it difficult to select suitable thermal storage container. In contrast, metals and alloys have higher thermal conductivity (ranging from 10 W/mK to 400 W/mK) and smaller volume expansion during phase transitions than molten salts [14,15]. As a result, the metals and alloys have received an increasing attention as new high-temperature PCMs.

Among the reported metallic PCMs, aluminum-silicon (Al-Si) alloys are recommended as the most potential solid-liquid PCMs for high temperature thermal energy storage applications owing to their suitable

phase change temperature range, high thermal energy storage capacity and good thermal stability. However, like other solid-liquid high temperature PCMs, the fluidity and high corrosion of the melted state still remain the challenges in their practical applications [6,13]. In order to simultaneously solve the above problems, the Al-Si alloys are usually encapsulated in the shell materials with high melting point to form composite PCMs. Fernandez et al. [15] summarized that metallic PCMs, including Al-Si alloys, can be encapsulated by ceramic or metal materials. For the ceramic encapsulation, the difference of thermal expansion will make the ceramic shell bear significant strain and eventually lead to fracture. Although metal encapsulation solves this problem, there are chances of diffusion corrosion leading to the formation of intermetallic. Therefore, various oxides are considered to be the most promising shell materials to encapsulate metallic PCMs.

He et al. [16] used Al_2O_3 to encapsulate the Al-12 wt%Si alloy and synthesized the Al_2O_3 shell layer by using aluminum sec-butoxide as a precursor to produce AlOOH, with a subsequent heat-oxidation treatment. They studied the structure and phase change characteristics of the composite PCM by varying the number of thermal cycling. The results showed that the prepared composite PCM had a high thermal storage capacity (307.21 J/g) and good thermal cycling stability. Nomura et al. [17] developed a two-step microencapsulation method, including the boehmite (AlOOH) coating and a heat-oxidation treatment, to prepared Al_2O_3 as the shell layer of the Al-25 wt%Si alloy PCM. The melting temperature and latent heat of the prepared composite PCM was 577 °C and 233 J/g, respectively. Sheng et al. [18] successfully prepared the Al-25 wt%Si/Al_2O_3 microencapsulated composite PCMs and the Al_2O_3 shell layer was prepared by three steps: the boehmite treatment in $Al(OH)_3$ supersaturated solution with adjustable pH values, the precipitation treatment and heat-oxidation. The results showed that the prepared microencapsulated composite PCM exhibited good thermal storage property and excellent thermal cycling stability.

From the earlier reports, it can be concluded that the Al-Si/Al_2O_3 microencapsulated composite PCMs were usually prepared as follows: the Al-Si alloy (with Al-12 wt%Si or Al-25 wt%Si) was used as the starting material, and the Al_2O_3 shell layer was generally synthesized by the AlOOH coating and heat-oxidation treatment. The Al-Si/Al_2O_3 composite PCMs with a high thermal storage capacity and good thermal cycling stability could be prepared by the above synthetic method. However, it is difficult to adjust the component of Al-Si alloy PCM during the preparation process of Al_2O_3 shell layer, so that only a specific melting temperature was observed in the reported Al-Si/Al_2O_3 composite PCMs. The melting temperature, corresponding to the thermal storage temperature, largely determines the actual application conditions of PCMs. Liu et al. [19] and Lai et al. [20] pointed out that the composite PCMs with adjustable melting temperature showed a broader application prospect than those with a particular melting temperature. Therefore, it is necessary to develop a method to prepare the Al-Si/Al_2O_3 composite PCMs with tunable melting temperature.

In this study, a novel and simple strategy was purposed to simultaneously achieve the Al_2O_3 shell preparation and Al-Si alloy composition adjustment of the composite PCMs, thereby obtaining the Al-Si/Al_2O_3 composite PCMs with tunable melting temperature. The developed procedure can be a break-through technique for preparing high temperature composite PCMs. To realize this novel concept, the raw Al powder was selected as the starting material and tetraethoxysilane (TEOS) as SiO_2 source, and the displacement reaction between SiO_2 and molten Al ($4Al + 3SiO_2 = 3Si + 2Al_2O_3$) was used to in-situ synthesize the Al-Si alloy PCM and Al_2O_3 shell. Meanwhile, the Al-Si alloy composition and Al_2O_3 shell thickness were tuned by altering the amount of TEOS added. The DSC analysis results showed that the melting temperature of prepared Al-Si/Al_2O_3 composite PCMs, depending on the Al-Si alloy composition, can be tuned from 574.0 °C to 641.4 °C, and the prepared composite PCMs exhibited a relatively high thermal storage capacity (from 248.6 J/g to 331.0 J/g).

2. Materials and methods

2.1. Materials

Aluminum powders (Al, purity: 99.9%) were purchased from Yuhang Aluminum co., Ltd., China. 3-Aminopropyl trimethoxysilane (APTMS, $C_6H_{17}NO_3Si$, AR), absolute ethanol (CH_3CH_2OH, AR), polyvinylpyrrolidone (PVP, $(C_6H_9NO)_n$, AR), tetraethoxysilane (TEOS, Si$(OC_2H_5)_4$, AR) and phenolic resin (PF, $(C_6H_6O \cdot CH_2O)_x$, AR) were purchased from Sinopharm co., Ltd., China.

2.2. Preparation of the Al-Si/Al_2O_3 composite PCMs

The Al-Si/Al_2O_3 composite PCMs were prepared as follows: 0.25 g of PVP was dissolved in 100 ml mixture of 5% deionized water and 95% absolute ethanol. Al powders (0.75 g) were dispersed in the above solution and stirred at 50 °C for 0.5 h. Then, 150 μl of APTMS was carefully dropwise added into the above solution and stirred at 50 °C for 1 h. This solution was labeled as solution A. The solution B was prepared as follows: 0.1 g of PF was dissolved in 100 ml absolute ethanol solution and then TEOS in varying quantities (3.9 g, 4.3 g, 4.7 g, 5.1 g) were added into the solution. After that, the solution B was carefully added dropwise into the solution A and stirred at 50 °C for 24 h. The samples were filtrated, dried, ground and calcined in an argon atmosphere (at 600 °C for 0.5 h and 1000 °C for 3 h). Finally, the products were ground and calcined in air to remove the excess carbon. The prepared composite PCMs in this study were labeled as CP_X, where X is the weight of TEOS added.

The preparation process of Al-Si/Al_2O_3 microencapsulated composite PCM and the chemical reactions that may occur during the preparation process [21–26] are shown in Fig. 1. As seen from Fig. 1, the preparation process of Al-Si/Al_2O_3 composite PCMs consisted of the formation of precursor shell on Al microspheres and the calcination process in an argon atmosphere. Specifically, the formation process of precursor shell was as follows: the surfaces of Al microspheres were firstly amino-functionalized by using APTMS as the coupling agent, and then the amino-functionalized Al microspheres were connected with the composites consisting TEOS and PF by the hydrogen bond interaction between NH_2 and Si-OH.

2.3. Characterization

The phase compositions of samples were studied by X-ray diffraction (XRD, D/MAX-Ultima IV, Bruker Corporation, USA). Scanning electron microscopy (SEM, SU70, Hitachi High-Technologies Corporation, Japan) was used to study the micro-structure of the prepared composite PCMs, while the elemental compositions and distribution were determined by energy dispersive spectroscopy (EDS). The phase change temperature and the latent heat of prepared composite PCMs were measured via differential scanning calorimetry (DSC, DSC404C, NETZSCH Corporation, Germany). Laser particle analyzer (LS-POP(9), OMEC Instruments Corporation, China) was used to examine the particle diameter distribution and average particle diameter of the samples. Fourier transform infrared spectrometer (FT-IR, Nicolet is10, Thermo Fisher Scientific Corporation, China) was used to verify the formation of shell layer on Al microspheres.

The thermal cycling test in ambient air was used to determine the thermal reliability and repeatable utilization property of the prepared composite PCMs. The thermal cycling test was conducted as follows: the prepared composite PCMs were loaded into the Al_2O_3 crucible and then placed into a muffle furnace. The thermal cycle test consisted of the melting and freezing process. Specifically, the samples were heated from room temperature to 30 °C above the melting temperature at a rate of 10 °C/min, held for 2 min, and then cooled to 500 °C at a rate of 10 °C/min. The above thermal cycle was repeated 20, 60, 100 times.
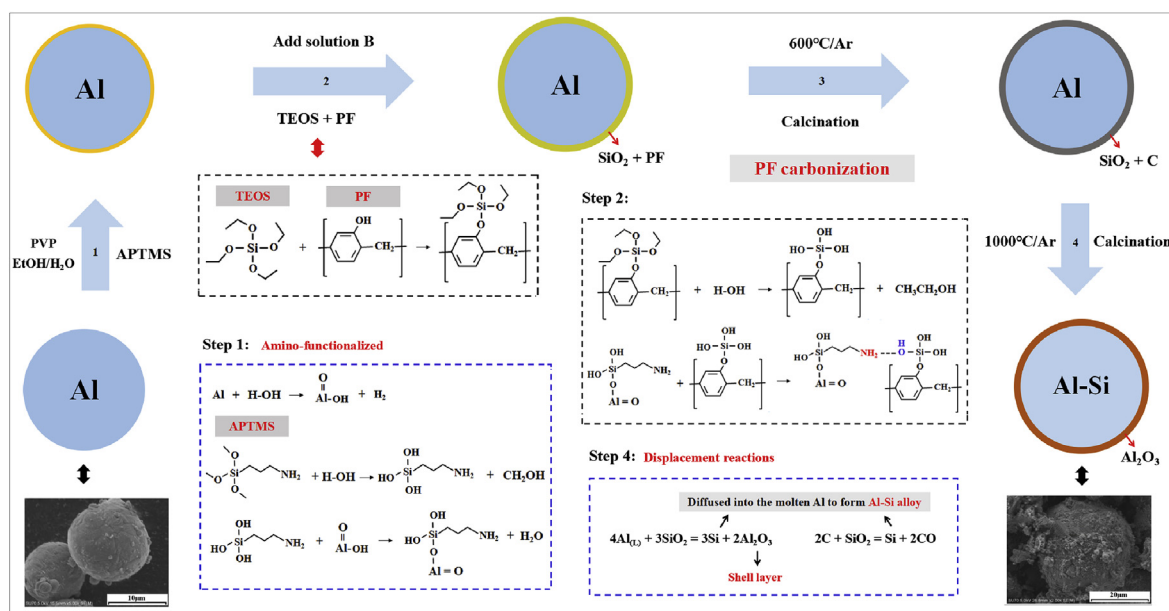
Fig. 1. Schematic diagram of the preparation process of Al-Si/Al$_2$O$_3$ composite PCM, Steps 1 and 2 correspond to the formation of precursor shell on the surface of amino-functionalized Al microspheres, Steps 3 and 4 represent the calcination process in an argon atmosphere.

3. Results and discussion

3.1. Structure characterization of the samples

The FT-IR analyzes the molecular structure and the chemical composition by using the absorption characteristics of infrared radiation at different wavenumbers. In this study, we used the FT-IR spectra to determine the formation of shell layer on Al microspheres. Fig. 2 (a) shows the FT-IR spectra of samples before calcination. According to Fig. 2 (a), there is no significant difference in the FT-IR spectra of samples in terms of shape and peak position. The characteristic peaks of Si-O were observed, indicating that TEOS was successfully loaded, hydrolyzed and condensed into SiO$_2$. The peak located at 1657 cm^{-1} was ascribed to the C=C stretching vibration of benzene ring in PF. The peak at around 3480 cm^{-1} was assigned to the –OH stretching vibration. It can be clearly seen from Fig. 2 (a) that the peaks intensities of Si-O and C=C increased significantly with the increasing addition of TEOS, suggesting that the precursor shell thickness composed of SiO$_2$ and PF markedly increased. Fig. 2 (b) shows the FT-IR spectra of

samples after calcination. As shown in Fig. 2 (b), a wide peak region at 571-813 cm^{-1} is observed, which can be ascribed to the Al-O stretching vibration. Compared with the FT-IR spectra of samples before calcination, the intensity of Si-O peak in the FT-IR spectra of samples after calcination decreased obviously, while that of Al-O stretching vibration peak increased significantly. This suggests that most of the SiO$_2$ in the precursor shell was converted into the Al$_2$O$_3$ after calcination.

The phase composition of the prepared composite PCMs was identified by XRD. Fig. 3 shows the XRD patterns of samples CP$_{3.9}$, CP$_{4.3}$, CP$_{4.7}$ and CP$_{5.1}$. According to Fig. 3, the composite PCMs were mainly composed of Al, Al$_2$O$_3$ and Si [28,29]. The presence of Al$_2$O$_3$ and Si diffraction peaks demonstrates that during the preparation process of composite PCMs, the displacement reaction between SiO$_2$ and molten Al occurred (4Al + 3SiO$_2$ = 3Si + 2Al$_2$O$_3$). Moreover, it can be also seen from Fig. 3 that the intensities of Al$_2$O$_3$ and Si diffraction peaks increased significantly with the increase in the addition of TEOS. In addition, a small SiO$_2$ diffraction peak at about 33° was observed in the XRD patterns of composite PCMs due to that a small amount of SiO$_2$ in the system was non-reactive.
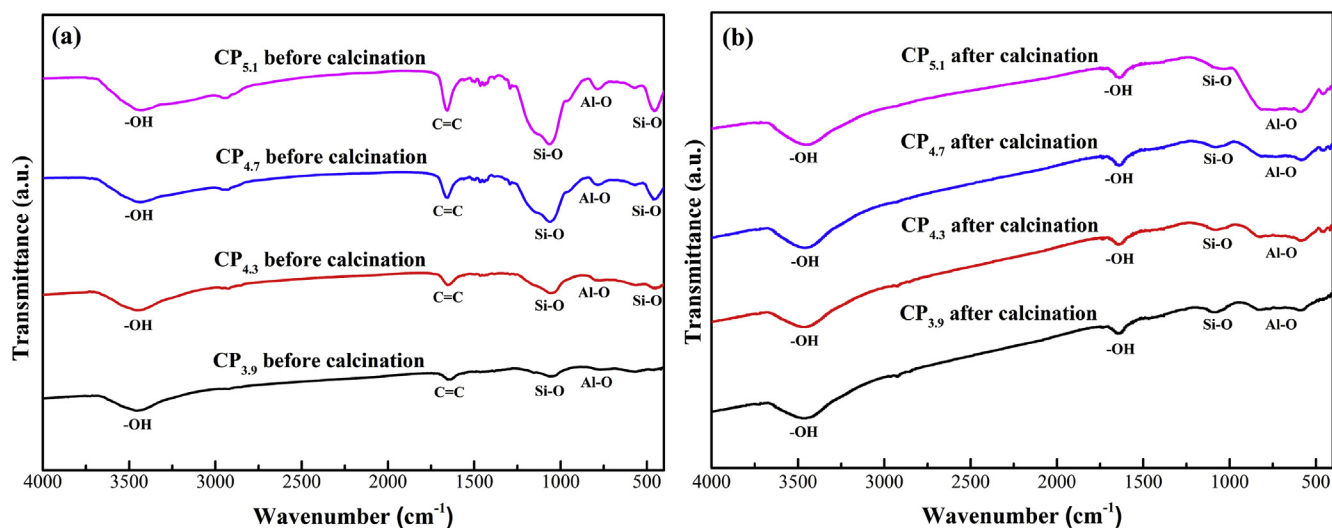

Fig. 2. FT-IR spectra of CP$_{3.9}$, CP$_{4.3}$, CP$_{4.7}$, CP$_{5.1}$ (a) before and (b) after calcination.

Fig. 3. XRD patterns of CP$_{3.9}$, CP$_{4.3}$, CP$_{4.7}$ and CP$_{5.1}$.

particle diameter of composite PCMs decreased with an increase in the addition of TEOS. Compared to the raw Al powders, the average particle diameter of samples CP$_{3.9}$, CP$_{4.3}$ and CP$_{4.7}$ increased significantly. The reason for the increase of particle diameter is that the particle diameter of composite PCMs was closely related to the precursor shell thickness of samples. During the preparation process of composite PCMs, the formed thin shell layer, depending on the amount of TEOS added, was unable to resist the thermal stress caused by the volume expansion of Al melting, which leaded to the partial rupture of the shell layer and the particle aggregation of prepared composite PCMs. The average particle diameter of CP$_{5.1}$ (35.7 μm) was close to that of raw Al particle (30.1 μm), suggesting that the sample CP$_{5.1}$ was well encapsulated and the shell layer of CP$_{5.1}$ was enough thick to prevent the molten Al from aggregation.

The SEM image of Al, CP$_{3.9}$, and CP$_{5.1}$ at a high magnification is respectively shown in Fig. 4 (d, e, f) in order to observe the microstructure of samples more clearly. According to Fig. 4 (d), the raw Al powders possessed a smooth surface, which was beneficial to combine with more water molecules to form Al-OH groups [27]. As shown in Fig. 4 (e, f), the surface of prepared composite PCMs was relatively rough and a number of small particles were detected on the surface. The energy dispersion spectrum (EDS) was used to further determine the shell layer element composition of CP$_{3.9}$ and CP$_{5.1}$. The analysis areas correspond to the purple rectangles in Fig. 4 (e) and (f), and the results are listed in Table 1. According to Table 1, the shell layer of CP$_{3.9}$ and CP$_{5.1}$ was mainly composed of Al and O elements. It was also observed that the content of Si in sample CP$_{5.1}$ was higher than that in sample CP$_{3.9}$, which is caused by the increase in the amount of TEOS added in sample CP$_{5.1}$. Furthermore, the elemental mapping of CP$_{3.9}$ and CP$_{5.1}$, respectively presented in Fig. 4(g–i) and Fig. S2, intuitively verified the

The morphology of the raw Al powders before and after encapsulation was observed by SEM. Fig. 4 (a, b, c) shows the SEM image of raw Al powders, CP$_{3.9}$, and CP$_{5.1}$, respectively, at a low magnification. The figure shows that most of the raw Al powders after encapsulation remain in an origin spherical shape, but the particle diameter changed obviously. The average particle diameter (AD) of samples Al, CP$_{3.9}$, CP$_{4.3}$, CP$_{4.7}$ and CP$_{5.1}$ was measured to be 30.1 μm, 130.8 μm, 90.1 μm, 58.2 μm and 35.7 μm, respectively, by laser particle analyzer (as given in Fig. S1). The results suggest that the average
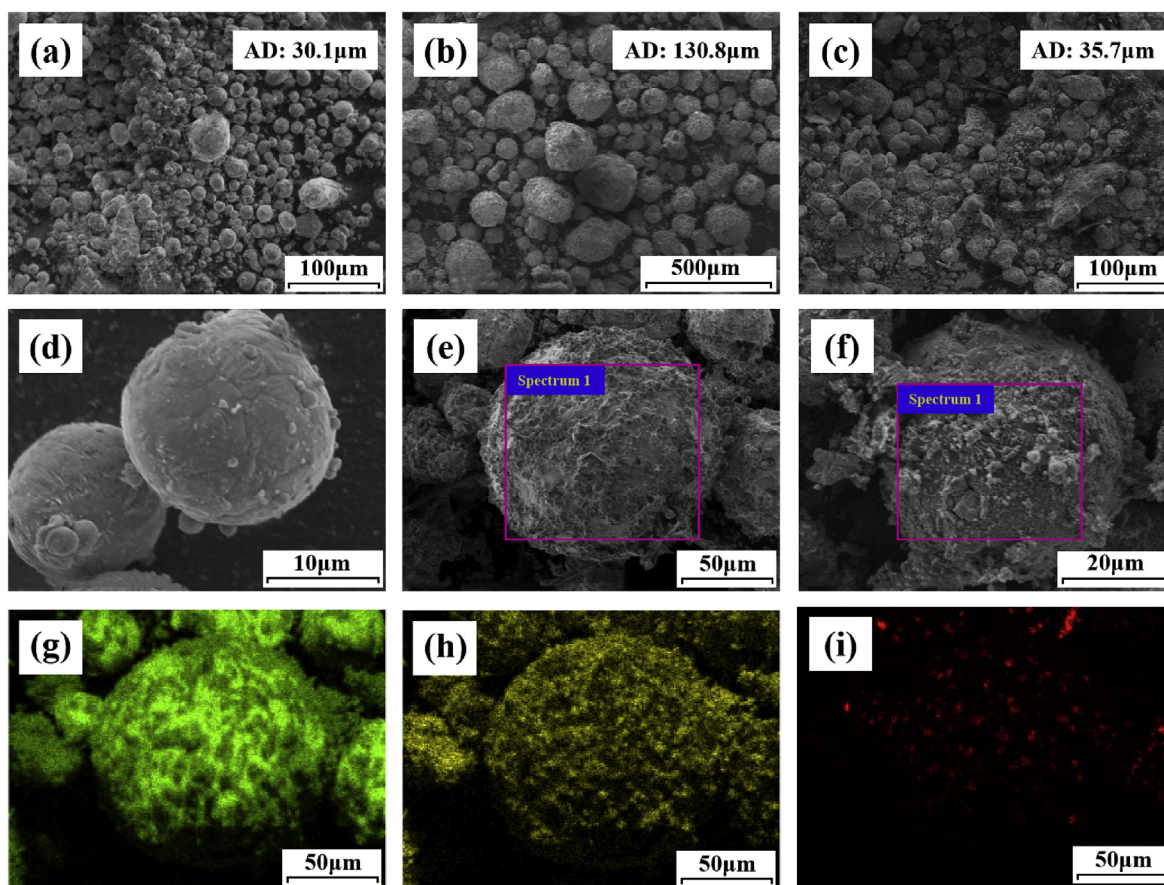

Fig. 4. SEM images of (a, b) raw Al powders; (c, d) CP$_{3.9}$; (e, f) CP$_{5.1}$ obtained at various magnifications, and (g) Al elemental mapping, (h) O elemental mapping, (i) Si elemental mapping of sample CP$_{3.9}$.

Table 1

Elemental composition of sample $CP_{3.9}$ and $CP_{5.1}$.

Element	$CP_{3.9}$ (at.%)	$CP_{5.1}$ (at.%)
O	52.36	51.45
Al	46.40	39.56
Si	1.24	8.99
Total	100.00	100.00

analysis results of EDS.

The SEM images of cracked sample $CP_{3.9}$, as shown in Fig. 5 (a, b), were used to observe the inner structure of prepared composite PCMs. According to Fig. 5 (a, b), the sample $CP_{3.9}$ exhibited a typical core-shell structure and a thin shell layer was clearly observed in the sample $CP_{3.9}$. Furthermore, it can be seen from the SEM image and elemental mapping of cross-sectional sample $CP_{3.9}$ [Fig. 5 (c-f)] that the core of sample $CP_{3.9}$ was composed of Al and a small amount of Si. The O element was principally distributed in the shell layer of particles, and the distribution of O element was not very uniform and continuous due to the uneven load of precursor shell. Additionally, the SEM images of cracked and cross-sectional sample $CP_{5.1}$, and elemental mappings are provided in Fig. S3. The similar results were obtained from Fig. S3. It is worth mentioning that the distribution density of O element in sample $CP_{5.1}$ was higher than that of sample $CP_{3.9}$, indicating that the shell layer of sample $CP_{5.1}$ was thicker than that of sample $CP_{3.9}$. It can be concluded from the FT-IR, XRD, SEM and EDS analysis results that the prepared microencapsulated composite PCMs consisted of Al-Si alloy core and Al_2O_3 shell layer.

3.2. Thermal storage property of prepared composite PCMs

The DSC heating and cooling curves of the prepared composite PCMs are respectively given in Fig. 6 (a) and (b), and their corresponding thermophysical properties are listed in Table 2. In the DSC heating curve of sample $CP_{3.9}$ and $CP_{4.3}$, there were two endothermic peaks, which correspond to the eutectic melting and alloy melting, respectively [20]. As seen from Fig. 6 (a), with the increase of Si content in the prepared composite PCMs, the alloy melting peak moves toward the lower temperature zone and the intensity of eutectic melting peak increased. For sample $CP_{4.7}$ and $CP_{5.1}$, only one endothermic peak was observed. Additionally, it can be seen from Fig. 6 (b) that the variation trend of the exothermic peak was consistent with that of endothermic peak.

As given in Table 2, the initial melting temperature (T_{im}) and peak melting temperature (T_{pm}) of the prepared composite PCMs can be adjusted from 574.0 °C to 641.4 °C and 585.9 °C–660.7 °C, respectively. The reason for the tunable melting temperature of the composite PCMs can be further illustrated by combining with the Al-Si binary phase diagram [Fig. 6 (c)]. According to Fig. 6 (c), the binary alloy systems melted or solidified within a temperature range, rather than at a particular temperature. The melting process of Al-Si binary alloy can be described as follows. When the system temperature [T_1, as shown in Fig. 6 (c)] was lower than the eutectic melting temperature of Al-Si alloy ($T_{Eutectic}$), the alloy was composed of α phase and Si phase. When the system temperature (T_2) was higher than the eutectic melting temperature, the Si phase of alloy transformed into the eutectic liquids. As the system temperature rose further above the liquidus temperature ($T_{Liquidus}$), the Al-Si alloy melted completely. Thus, the melting temperature of Al-Si binary alloy included the eutectic temperature and liquidus temperature of Al-Si alloy. As shown in Fig. 6 (c), the eutectic temperature of Al-Si alloy was a specific temperature, while the liquidus temperature of Al-Si alloy varied with the content of Si. Therefore, the melting temperature of prepared composite PCMs can be adjusted by altering the Al-Si alloy component. Furthermore, the Al-Si alloy composition of the prepared composite PCMs can be estimated by their liquidus temperature. Kousksou et al. [30] and Wang et al. [31] demonstrated that the intersection of the tangent line at the point when the curve started to deviate from the baseline and the tangent line at the maximum slope of the curve was closest to the equilibrium temperature of thermodynamics. As a result, this point is determined by extrapolation method as the initial point of the endothermic peak. As shown in Table 2, the liquidus temperature of sample $CP_{3.9}$ and $CP_{4.3}$ corresponded to the initial melting temperature of secondary endothermic peak, and was measured to be respectively 641.4 °C and 624.0 °C, which indicates that the Si content of sample $CP_{3.9}$ and $CP_{4.3}$ was around 2.7% and 5.1%, as labeled in Fig. 6 (c). For the sample $CP_{4.7}$ and $CP_{5.1}$, only one endothermic peak was observed, suggesting that the alloy composition of $CP_{4.7}$ and $CP_{5.1}$ was close to the eutectic composition of Al-Si alloy (11.7% Si). To further estimate the Al-Si alloy composition, the liquidus temperature of sample $CP_{4.7}$ and $CP_{5.1}$ was approximately the peak melting temperature of endothermic peak [32] (586.2 °C for $CP_{4.7}$, and 585.9 °C for $CP_{5.1}$). Thus, the Si content of sample $CP_{4.7}$ and $CP_{5.1}$ was about 10.4% and 12.6%, respectively.

The melting latent heat of samples $CP_{3.9}$, $CP_{4.3}$, $CP_{4.7}$ and $CP_{5.1}$ is
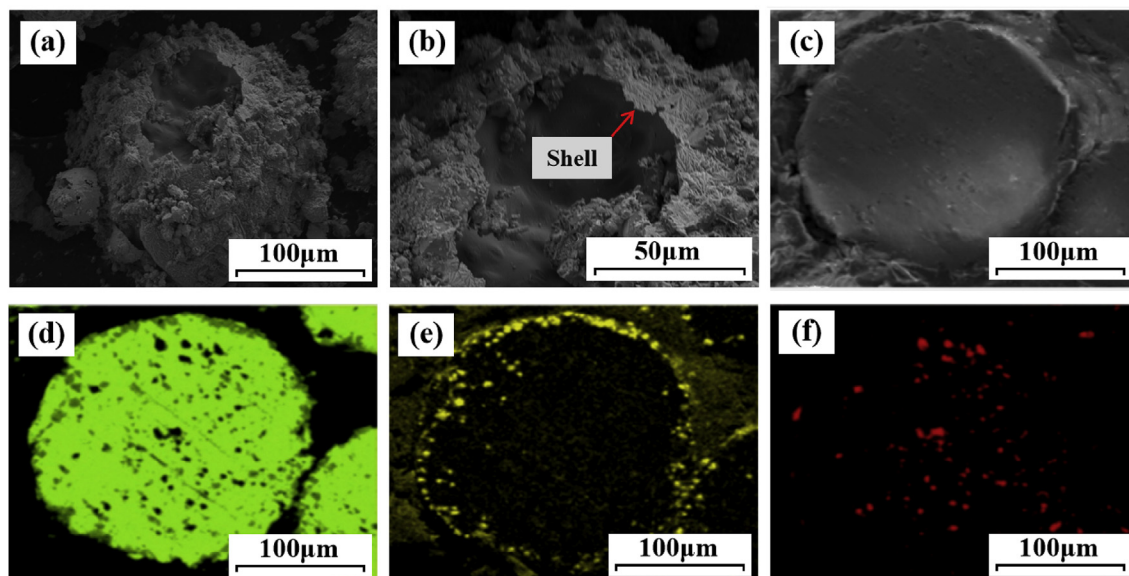

Fig. 5. SEM images of (a, b) cracked sample $CP_{3.9}$; (c) cross-sectional sample $CP_{3.9}$ and (d) Al elemental mapping; (e) O elemental mapping; (f) Si elemental mapping.
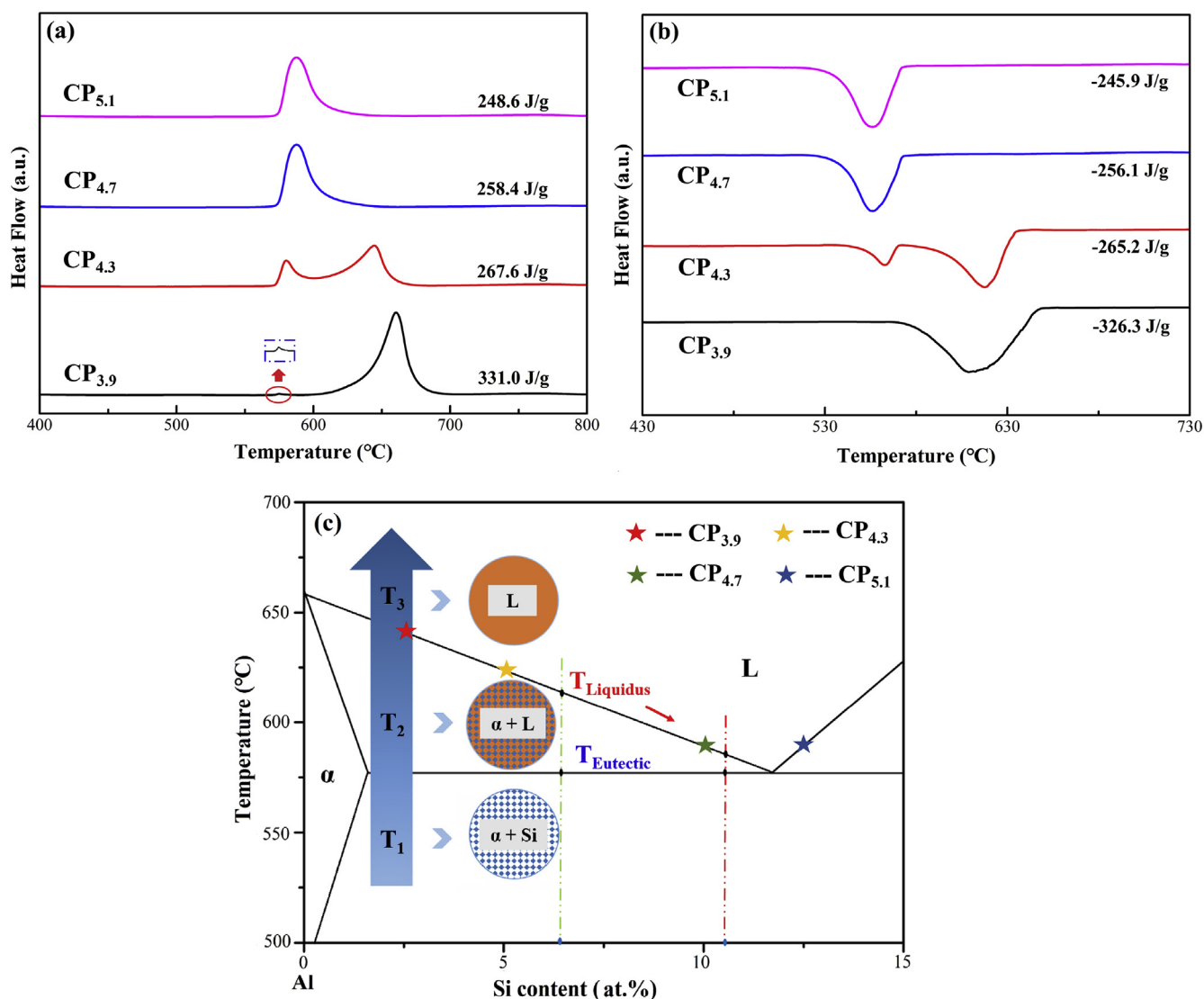
Fig. 6. (a) DSC heating curves; (b) DSC cooling curves of samples CP$_{3.9}$, CP$_{4.3}$, CP$_{4.7}$ and CP$_{5.1}$; and (c) partial phase diagram of Al-Si binary alloys whose liquidus temperature varies with the content of Si.

331.0 J/g, 267.6 J/g, 258.4 J/g and 248.6 J/g, respectively. The results show that the melting latent heat of the prepared composite PCMs decreased with the increase in the Si content. The reason of melting latent heat reduction is that the melting latent heat in the core-shell composite PCMs was attributed to the melting of the Al-Si alloy. Therefore, in a unit mass composite PCMs, the higher the content of core PCM, or the thinner the thickness of shell layer, the higher the melting latent heat value, and vice versa. Combined with the XRD and EDS analysis results, the shell layer thickness of prepared composite PCM increased with an increase in the Si content. Thus, the melting latent heat of the prepared composite PCMs decreased with an increase in the Si content. Similarly, the sample CP$_{3.9}$ showed the highest

crystallization latent heat (326.3 J/g) among the prepared composite PCMs.

The melting temperature and melting latent heat of the prepared composite PCMs in this study were compared with those of reported relevant composite PCMs in literature (as given in Table 3). According to Table 3, the prepared Al-Si/Al$_2$O$_3$ composite PCMs in this study not only exhibited a relatively high melting latent heat, but also demonstrated a wide melting temperature adjustment range. The melting temperature adjustability of composite PCMs provided an additional flexibility in different working temperature conditions. Therefore, the prepared composite PCMs have a broader application prospect for various industrial systems under different working temperature

Table 2
Mass of before (M$_1$) and after (M$_2$) encapsulation, initial melting temperature (T$_{im}$), peak melting temperature (T$_{pm}$), melting latent heat (H$_m$), initial crystallization temperature (T$_{ic}$), peak crystallization temperature (T$_{pc}$) and crystallization latent heat (H$_c$) of samples.

Samples	M$_1$ (g)	M$_2$ (g)	T$_{im}$ (°C)	T$_{pm}$ (°C)	H$_m$ (J/g)	T$_{ic}$ (°C)	T$_{pc}$ (°C)	H$_c$ (J/g)
CP$_{3.9}$	0.751	0.809	573.9/641.4	575.2/660.7	331.0	646.3	619.3	−326.3
CP$_{4.3}$	0.752	0.852	573.5/624.0	580.0/644.9	267.6	569.5/632.5	562.8/617.3	−265.2
CP$_{4.7}$	0.748	0.933	574.0	586.2	258.4	572.2	556.2	−256.1
CP$_{5.1}$	0.750	0.961	574.2	585.9	248.6	572.4	556.1	−245.9

Table 3
Thermal properties comparison of prepared composite PCMs in this study with those of reported relevant composite PCMs in literature.

Composite PCMs	Melting temperature (°C)	Melting latent heat (J/g)	References
Al/Al_2O_3	663.5	312.7–351.8	33
Al-12 wt% Si/Al_2O_3	-	307.21	16
Al-25 wt% Si/Al_2O_3	579	233	17
Al-25 wt% Si/Al_2O_3	577	181–251	18
Al-Si/Al_2O_3	574.0–641.4	248.6–331.0	This study
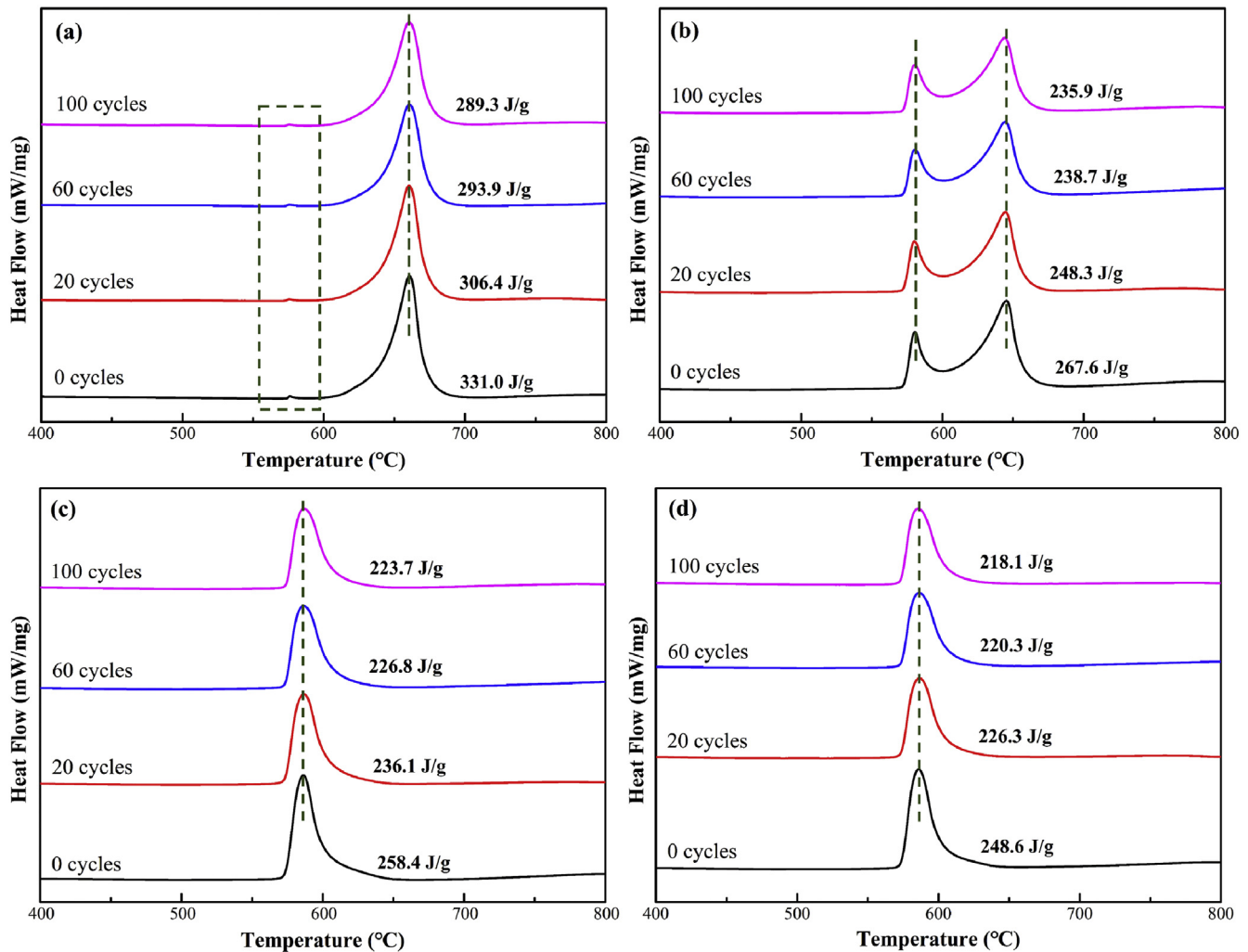
Fig. 7. DSC heating curves of the prepared (a) $CP_{3.9}$; (b) $CP_{4.3}$; (c) $CP_{4.7}$, and (d) $CP_{5.1}$ after 0, 20, 60, 100 thermal cycles.

conditions.

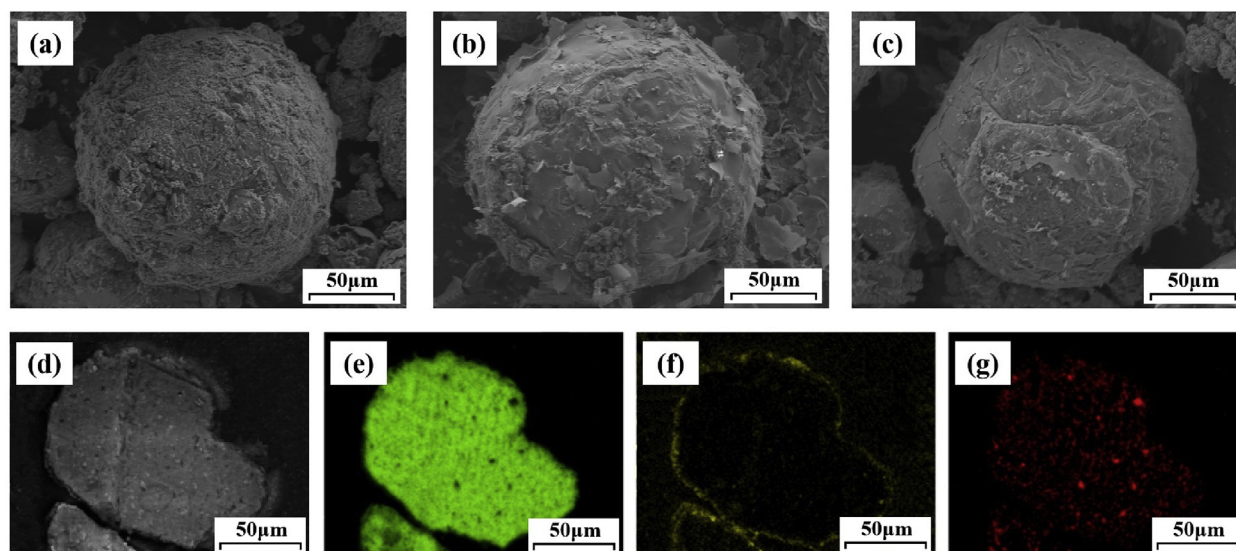### 3.3. Thermal cycling stability of prepared composite PCMs

The prepared composite PCMs are required to possess good thermal cycling stability and repeatable utilization property, since they are bound to go through many thermal cycles in practical applications. Fig. 7 shows the DSC heating curves of the prepared composite PCMs after 0, 20, 60 and 100 thermal cycles. The melting temperature of composite PCMs remained almost unchanged after thermal cycling (as shown in Fig. 7). The melting latent heat of prepared composite PCMs after different thermal cycles is given in Table 4. As seen from Table 4, although the melting latent heat of the prepared composite PCMs after 100 thermal cycles decreased, it was still relatively high (ranging from 218.1 J/g to 289.3 J/g). The total melting latent heat loss after 100 thermal cycles of $CP_{3.9}$, $CP_{4.3}$, $CP_{4.7}$ and $CP_{5.1}$ was 41.7 J/g, 31.7 J/g,

Table 4
Melting latent heat of composite PCMs after different thermal cycles.

Samples	0 cycles (J/g)	20 cycles (J/g)	60 cycles (J/g)	100 cycles (J/g)	Total loss amount (J/g)
$CP_{3.9}$	331.0	306.4	293.9	289.3	41.7
$CP_{4.3}$	267.6	248.3	238.7	235.9	31.7
$CP_{4.7}$	258.4	236.1	226.8	223.7	34.7
$CP_{5.1}$	248.6	226.3	220.3	218.1	30.5

34.7 J/g and 30.5 J/g, respectively. The observed melting latent heat decrease can be ascribed to the oxidation of surface unencapsulated Al-Si. It can be also seen from Table 4 that the melting latent heat loss of composite PCMs obviously decreased with the increase in the thermal cycles and there was almost no melting latent heat loss in the prepared composite PCMs from 60 to 100 thermal cycles. This suggests that the

Fig. 8. SEM images of CP$_{3.9}$ after (a) 20 cycles; (b) 60 cycles; (c) 100 cycles; (d) SEM image of cross-sectional CP$_{3.9}$ after 100 cycles and (e) Al element mapping; (f) O element mapping; (g) Si element mapping.

cracks caused by incomplete encapsulation can be self-repaired by the oxidation of inner Al-Si during the thermal cycling [33,34]. Therefore, the prepared composite PCMs exhibited a good thermal stability, repeatable utilization property and certain shell layer self-repairing ability in the working temperature range.

To further evaluate the thermal cycling stability of the prepared composite PCMs (i.e., the sample CP$_{3.9}$), we also determined the changes of microstructure after different thermal cycles. The SEM images of sample CP$_{3.9}$ after 20, 60 and 100 thermal cycles are shown in Fig. 8 (a), (b) and (c), respectively. It can be clearly observed from Fig. 8(a–c) that the shell layer of sample CP$_{3.9}$ generally became smoother and denser with the increase of thermal cycle numbers. Fig. 8(d–g) shows the SEM image and elemental mapping of cross-sectional CP$_{3.9}$ after 100 thermal cycles. As given in the O elemental mapping, a relatively dense and continuous Al$_2$O$_3$ shell layer was formed in the sample CP$_{3.9}$ after 100 thermal cycles. It can be concluded from Fig. 5(c–f) and Fig. 8(d–g) that the sample CP$_{3.9}$ possessed a certain shell layer self-repairing ability during the thermal cycling, when compared to the sample before the thermal cycle. Furthermore, it is inevitable that a small number of samples would break during the thermal cycle. The SEM images of cracked sample CP$_{3.9}$ after 20 and 100 thermal cycles were given in Fig. S4.

4. Conclusions

In this study, a novel method was purposed to successfully prepare the Al-Si/Al$_2$O$_3$ microencapsulated composite PCMs with tunable melting temperature. This preparation method not only achieved the in-situ synthesis of the Al-Si alloy PCM and Al$_2$O$_3$ shell layer, but also realized the adjustment of Al-Si alloy composition and Al$_2$O$_3$ shell thickness by altering the addition of TEOS. To demonstrate the melting temperature adjustability of prepared composite PCMs, we prepared four composite PCMs with different TEOS additions. The DSC analysis results showed that the melting temperature of prepared composite PCMs could be adjusted from 574.0 °C to 641.4 °C by altering the Al-Si alloy composition. Moreover, the prepared composite PCMs exhibited an excellent high thermal storage capacity (248.6 J/g to 331.0 J/g), thermal stability, repeatable utilization property and certain self-repairing ability in the working temperature range. Thus, the prepared composite PCMs are expected to be preferential potential candidates to improve the energy efficiency of various systems under different working temperature conditions. Additionally, the synthetic strategy

used in the Al-Si/Al$_2$O$_3$ can be extended to other alloy powder systems, which opens up a novel reference method to design high temperature microencapsulated composite PCMs with tunable melting temperature.

Appendix A. Supplementary data

Supplementary data to this article can be found online at https://doi.org/10.1016/j.solmat.2019.110166.

References

[1] A. Sharma, V. Tyagi, C. Chen, D. Buddhi, Review on thermal energy storage with phase change materials and applications, Renew. Sustain. Energy Rev. 13 (2009) 318–345.

[2] M. Kenisarin, K. Mahkamov, Solar energy storage using phase change materials, Renew. Sustain. Energy Rev. 11 (2007) 1913–1965.

[3] X. Li, H. Wei, X. Lin, X. Xie, Preparation of stearic acid/modified expanded vermiculite composite phase change material with simultaneously enhanced thermal conductivity and latent heat, Sol. Energy Mater. Sol. Cells 155 (2016) 9–13.

[4] H. Wei, X. Li, Preparation and characterization of a lauric-myristic-stearic acid/Al$_2$O$_3$-loaded expanded vermiculite composite phase change material with enhanced thermal conductivity, Sol. Energy Mater. Sol. Cells 166 (2017) 1–8.

[5] R. Fukahori, T. Nomura, C. Zhu, N. Sheng, N. Okinaka, T. Akiyama, Macroencapsulation of metallic phase change material using cylindrical-type ceramic containers for high-temperature thermal energy storage, Appl. Energy 170 (2016) 324–328.

[6] S. Khare, M. Dell Amico, C. Knight, S. McGarry, Selection of materials for high temperature latent heat energy storage, Sol. Energy Mater. Sol. Cells 107 (2012) 20–27.

[7] H. Wei, X. Xie, X. Li, X. Lin, Preparation and characterization of capric-myristic-stearic acid eutectic mixture/modified expanded vermiculite composite as a form-stable phase change material, Appl. Energy 178 (2016) 616–623.

[8] S. Guillot, A. Faik, A. Rakhmatullin, J. Lambert, E. Veron, P. Echegut, Corrosion effects between molten salts and thermal storage material for concentrated solar power plants, Appl. Energy 94 (2012) 174–181.

[9] N. Gokon, S. Nakamura, T. Hatamachi, T. Kodama, Steam reforming of methane using double-walled reformer tube containing high-temperature thermal storage Na$_2$CO$_3$/MgO composites for solar fuel production, Energy 68 (2014) 773–782.

[10] H. Tian, W. Wang, J. Ding, X. Wei, M. Song, J. Yang, Thermal conductivities and characteristics of ternary eutectic chloride/expanded graphite thermal energy storage composites, Appl. Energy 148 (2015) 87–92.

[11] Y. Tian, C. Zhao, A review of solar collectors and thermal energy storage in solar applications, Appl. Energy 104 (2013) 538–553.

[12] M. Liu, W. Saman, F. Bruno, Review on storage materials and thermal performance enhancement techniques for high temperature phase change thermal storage

systems, Renew. Sustain. Energy Rev. 16 (2012) 2118–2132.

[13] M. Kenisarin, High-temperature phase change materials for thermal energy storage, Renew. Sustain. Energy Rev. 14 (2010) 955–970.

[14] J. Liu, X. Wang, D. Zeng, G. Saito, D. Hanzaki, T. Hiraki, T. Akiyama, Microencapsulated phase change materials with high heat capacity and high cyclic durability for high-temperature thermal energy storage and transportation, Appl. Energy 188 (2017) 9–18.

[15] A. Fernandez, G. Barreneche, M. Belusko, M. Segarra, F. Bruno, L. Gabeza, Considerations for the use of metal alloys as phase change materials for high temperature applications, Sol. Energy Mater. Sol. Cells 171 (2017) 275–281.

[16] F. He, G. Song, X. He, C. Sui, M. Li, Structural and phase change characteristics of inorganic microencapsulated core/shell Al-Si/Al_2O_3 micro-particles during thermal cycling, Ceram. Int. 41 (2015) 10689–10696.

[17] T. Nomura, N. Sheng, C. Zhu, G. Saito, D. Hanzaki, T. Hiraki, T. Akiyama, Microencapsulated phase change materials with high heat capacity and high cyclic durability for high-temperature thermal energy storage and transportation, Appl. Energy 188 (2017) 9–18.

[18] N. Sheng, C. Zhu, G. Saito, T. Hiraki, M. Haka, Y. Hasegawa, H. Sakai, T. Akiyama, T. Nomura, Development of a microencapsulated Al-Si phase change material with high-temperature thermal stability and durability over 3000 cycles, J. Mater. Sci. 6 (2018) 18143–18153.

[19] M. Liu, Y. Ma, H. Wu, R. Wang, Metal matrix-metal nanoparticle composites with tunable melting temperature and high thermal conductivity for phase-change thermal storage, ACS Nano 9 (2015) 1341–1351.

[20] C. Lai, S. Lin, Y. Chu, C. Chang, Y. Chueh, Tunable endothermic plateau for enhancing thermal energy storage obtained using binary metal alloy particles, Nano Energy 25 (2016) 218–224.

[21] K. Vrancken, E. Casteleyn, K. Possemiers, V. Van der, E. Vansant, Modelling of the reaction-phase interaction of γ-Aminopropyltriethoxysilane with silica, J. Chem. Soc. 89 (1993) 2037–2040.

[22] K. Vrancken, K. Possemiers, V. Van der, E. Vansant, Surface modification of silica gels with aminoorganosilanes, Colloids Surf., A 98 (1995) 235–341.

[23] G. Wang, F. Yan, Z. Teng, W. Yang, T. Li, The surface modification of silica with

APTS, Prog. Chem. 18 (2006) 238–345.

[24] L. Pathak, D. Bandyopadhyay, S. Srikanth, S. Das, P. Ramachandrarao, Effect of heating rates on the synthesis of Al_2O_3-SiC composites by the self-propagating high-temperature synthesis (SHS) technique, J. Am. Ceram. Soc. 84 (2001) 915–920.

[25] N. Yoshikawa, A. Kikuchi, S. Taniguchi, Anomalous temperature dependence of the growth rate of the reaction layer between silica and molten aluminum, J. Am. Ceram. Soc. 85 (2002) 1827–1834.

[26] N. Lin, Y. Han, J. Zhou, K. Zhang, T. Xu, Y. Zhu, Y. Qian, A low temperature molten salt process for aluminothermic reduction of silicon oxides to crystalline Si for Li-ion batteries, Energy Environ. Sci. 8 (2015) 3187–3191.

[27] F. He, C. Sui, X. He, M. Li, Inorganic microcapsulated core-shell structure of Al-Si alloy micro-particles with silane coupling agent, Ceram. Int. 40 (2014) 6865–6874.

[28] H. Wang, Y. Li, T. Zhu, S. Sang, Q. Wang, Microstructures and mechanical properties of Al_2O_3-C refractories with addition of microcrystalline graphite, Ceram. Int. 40 (2014) 11139–11148.

[29] T. Chanadee, Experimental studies on self-propagating high-temperature synthesis of Si-SiC composite from reactants of SiO_2 derived from corn cob ash/C/Mg, J. Australas. Ceram. Soc. 53 (2017) 245–252.

[30] T. Kouskou, T. EI Rhafiki, M. Mahdaoui, P. Bruel, Y. Zeraouli, Crystallization of supercooled PCMs inside emulsions: DSC applications, Sol. Energy Mater. Sol. Cells 107 (2012) 28–36.

[31] H. Wang, S. Lu, Study on thermal properties of phase change material by an optical DSC system, Appl. Therm. Eng. 60 (2013) 132–136.

[32] T. Omori, J. Sato, K. Shinagawa, I. Ohnuma, K. Oikawa, R. Kainuma, K. Ishida, Experimental determination of phase equilibria in the Co-Cr-Ni system, J. Phase Equilibria Diffusion 35 (2014) 178–185.

[33] K. Li, X. Cheng, N. Li, X. Zhu, Y. Wei, K. Zhai, H. Wang, A yolk/shell strategy for designing hybrid phase change materials for heat management in catalytic reactions, J. Mater. Sci. 5 (2017) 24232–24246.

[34] N. Sheng, C. Zhu, H. Sakai, T. Akiyama, T. Nomura, Synthesis of Al-25wt%Si@Al_2O_3@Cu microcapsules as phase change materials for high temperature thermal energy storage, Sol. Energy Mater. Sol. Cells 191 (2019) 141–147.